Distance Protection for Lines Terminated by Inverter-Based Resources Compatible With Various Inverter Control Schemes

Yuhao Xie, *Student Member, IEEE*, Xinchen Zou, *Student Member, IEEE*, Mengzhao Duan, *Student Member, IEEE*, Feilong Fan, *Member, IEEE*, Haoyu Wang, *Senior Member, IEEE*, and Yu Liu, *Senior Member, IEEE*

***Abstract*—For lines terminated by inverter based resources (IBRs), the performance of the legacy distance relay could be affected by the characteristics of IBRs during faults. Improved distance relays in the existing literature often rely on communication from the remote end or specific IBR control strategies, limiting the compatibility of these relays. This article proposes a distance protection method at the IBR side of the line. First, the sequence equivalent circuits of IBRs are treated as three unavailable boxes. Next, the proposed method combines the information within multiple the sequence networks, to accurately consider the impact of fault resistance and remote end infeed current. Finally, the unknown fault distance is analytically solved as a root of the quadratic equation. The proposed method does not have specific assumption on IBR control schemes, step-up transformer winding connections, or branches at the local bus, and can therefore work in power systems with various grid codes. Moreover, the proposed method is compatible with present phasor data acquisition systems at local terminal and does not require remote end information. Simulations, hardware experiments and field data experiments demonstrate the effectiveness of the proposed distance protection.**

***Index Terms*—Distance relay, inverter based resources (IBRs), inverter control schemes, line protection.**

I. Introduction

RENEWABLES are typically connected to the power grid in the form of inverter based resources (IBRs). The characteristics of IBRs are quite different from those of synchronous generators (SGs) [1]. As a result, for transmission lines terminated by IBRs, line protection schemes encounter a series of challenges [2]. Line protection includes overcurrent protection [3], distance protection [4], [5], traveling wave-based protection [6], [7], current differential protection [8], [9], dynamic state estimation-based protection [10], [11], pilot protection [12], and so on. Among them, line distance protection is a widely applied single-ended scheme and will be the focus of this article.

Recent studies evaluate the impact of IBRs on the line relay. It has been shown that the current amplitude and phase angle of IBR side is affected by low-voltage ride-through (LVRT) scheme [13]. As a result, the weak-infeed and controlled source feature [14] could cause malfunction of IBR side legacy distance protection [15]. Furthermore, various control strategies of inverter will also affect the effectiveness of relay and make protection design more complicated [16], [17].

To overcome above challenges, various improved distance relay schemes are proposed to mitigate the effect of IBRs. One group of methods use information brought by the additional measurements or communication. For example, a time domain relay is proposed to achieve the source-independent distance protection [18]. The method requires measurements with a high sampling rate of tens of kHz to several MHz. In [19], a protection with an adaptive zone setting is proposed. The method uses IBR operating parameters and remote end source impedance to mitigate the impact of fault resistance. In [20], an adaptive distance relay is proposed using remote end source impedance. These methods improve the reliability of distance protection; however, extra measurement and communication hardware could be required.

Therefore, researchers proposed another group of distance protection schemes compatible with present data acquisition (local terminal phasor measurements). These methods are based on the assumptions on the specific control strategy of IBRs or system topology, to simplify the equations during the faults. The method in [21] assumes that the fault current is in phase with the current at the relay location, in negative and zero sequence networks, respectively. However, this assumption depends on the control strategy of IBRs. The method in [22] assumes that the inverter control strategy eliminates the negative sequence current. However, since IEEE Std 2800-2022 [17] suggests injecting negative sequence current during asymmetric faults, the reliability of the method is affected. For IBRs injecting negative sequence current, reference [23] proposes a method applying the negative sequence model to estimate fault location, but the precision still depends on details of IBR control schemes. Active control-based methods adjust the control scheme of IBRs during

Received 13 November 2024; revised 17 February 2025 and 18 April 2025; accepted 15 May 2025. Date of publication 25 July 2025; date of current version 21 November 2025. This work was supported by the National Natural Science Foundation of China under Grant 52377114. *(Corresponding author: Y. Liu.)*

Yuhao Xie, Xinchen Zou, Mengzhao Duan, Haoyu Wang, and Yu Liu are with ShanghaiTech University, Shanghai 201210, China (e-mail: liuyu@shanghaitech.edu.cn).

Feilong Fan is with Shanghai Jiao Tong University, Shanghai 200240, China.

Digital Object Identifier 10.1109/TIE.2025.3577310

faults, to enable reliable operation of the legacy relays. For example, references [24], [25] regulate the current phase angles during faults, while method [26] injects specific harmonic currents by adjusting IBR control during faults, making legacy distance relay effective. Overall, the effectiveness of these improved distance protection schemes typically relies on the specific control strategy of IBRs.

In practical power systems, distance relay is typically deployed without communication from the remote end. As a result, the relay designs using remote end information [18], [19], [20] are not quite attractive to field engineers. In addition, installed IBRs have different control strategies for different manufactures and grid codes. Sometimes, the detailed control strategies are even not available for utilities. This means the IBR control strategies may not fully meet the specific assumptions for distance relay design [21], [22], [23]. In addition, adjusting IBR control strategy of existing devices [24], [25], [26] is also difficult in practice. These facts could also cause applicability issues for these distance relays in practice. As a result, there still exists a clear research gap: how to design a distance relay that is compatible with various IBR control strategies and grid codes, and at the same time works with present data acquisition systems at the local terminal.

To merge this research gap, this article proposes a line distance protection method at the IBR side of the line. The proposed method only requires three phase voltage and current phasor measurements at the local end, and is compatible with various IBR control schemes. The proposed method carefully considers the impact of IBRs and fault resistances on single ended relay. Specifically, with accurate consideration of remote end infeed when calculating the fault current, the fault distance can be analytically estimated to ensure correct and fast operation of distance relay. The main contributions of the article are summarized as below

1) The proposed method fully adopts the information within multiple sequence networks, and derives the analytical expression of the fault distance as a root of the quadratic equation, independent of infeed currents from the remote end and fault resistances.
2) The proposed method adopts unavailable box models for IBRs during derivation; therefore, it is compatible with various IBR control schemes, grid codes, transformer winding connections for different power systems.
3) The proposed method is only based on phasor measurements at the local terminal before and during the fault, and can be implemented using present data acquisition in practice without communication from the remote end.
4) The proposed method demonstrates improved reliability compared to existing distance protection schemes, with simulation, hardware experiments, and field data experiments.

The remainder of the article is organized below. Section II presents the scheme of proposed distance protection. Section III demonstrates the reliability and compatibility of the proposed method via simulation. Section IV discusses the advantages of the proposed method compared to existing ones with operating scenarios. Sections V and VI present hardware and field data experimental results. Section VII concludes the article.

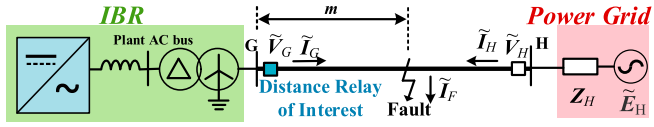

Fig. 1. Example transmission line system terminated by IBR.

II. Principle of Proposed Distance Protection

A. Problem Statement

An example transmission system terminated by IBR is shown in Fig. 1. The IBR is connected to the rest of the power grid through a transmission line G–H, where m is the distance to fault position. The figure shows a widely used Δ-YN connected step-up transformer as an example, but the derivation is applicable to transformers with other winding connections. The distance relay of interest is the relay at terminal G, which should trip internal faults within line GH.

Legacy distance protection issues trip signals by checking whether the apparent impedance "seen" by the relay, i.e., $Z_{\text{app}} = \tilde{V}_{G\varphi}/\tilde{I}_{G\varphi}$, enters the operating zone, where $\tilde{V}_{G\varphi}$ and $\tilde{I}_{G\varphi}$ have different expressions for various fault types [1].

In some fault cases, the fault may have a nonnegligible fault resistance R_F, causing a considerable voltage drop. As a result, an additional apparent impedance will occur, jeopardizing the performance of the distance relay [2]. For conventional grid that both line ends are dominated by SGs, $\tilde{I}_{G\varphi}$ and $\tilde{I}_{F\varphi}$ are usually with small phase angle differences [28]. Therefore, the additional apparent impedance contributed by the fault resistance is almost resistive. In fact, legacy distance protection with quadrilateral operating zone is widely adopted, which improves the robustness of the distance protection against the fault resistance in conventional grids.

However, due to the week infeed characteristics of IBRs, the grid side (the right side in Fig. 1) provides the majority of the fault current $\tilde{I}_F$. In addition, $\tilde{I}_{G\varphi}$ and $\tilde{I}_{F\varphi}$ are typically not in phase due to LVRT of IBRs [13]. As a result, the imaginary part of additional apparent impedance caused by the fault resistance could be huge [1], which could result in mal-operation of the legacy distance relay at IBR side and affect the protection reliability. Other relay designs such as memory-polarized relays also face similar challenges [29].

B. Sequence Network and Fault Current Analysis

The positive, negative, and zero sequence networks are the basis of fault analysis and protection design. The power grid side, which is dominated by synchronous generators, can be modelled as Thevenin equivalent circuits, with the constant voltage source for the positive sequence ($\tilde{E}_{H1}$) and constant impedances for all three sequences (Z_{H1}, Z_{H2}, and Z_{H0}) [18].

However, the IBR models are much more complicated, and are based on the control schemes and system topologies. For example, the negative sequence of IBR can be modeled as an open circuit when the control scheme completely suppresses the negative sequence current [21], [22]. The negative sequence current injection scheme will introduce an equivalent source in the negative sequence network [23], [24]. Moreover, in typical

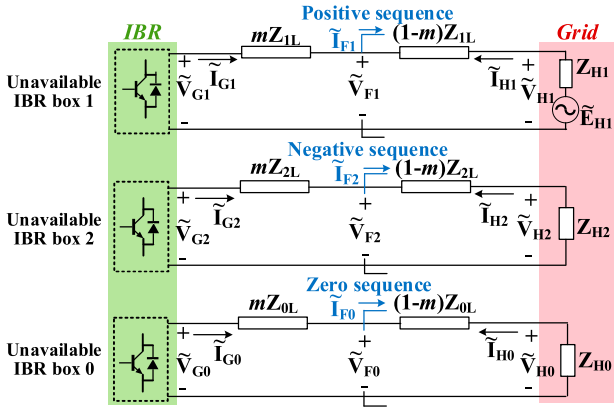

Fig. 2. Sequence network models of the system with IBR.

scenarios where Δ-YN step-up transformers are adopted to prevent overcurrent damage for IBRs during line faults, the zero sequence equivalent circuit of IBR only includes the zero sequence impedance of transformer [24]. In scenarios where other transformer winding connections are utilized [30], the zero sequence IBR model becomes more complicated. Finally, the equivalent circuit is also different for grid following (GFL) and grid forming (GFM) control schemes of IBR. The GFL inverter typically presents current source characteristics [31], and the GFM inverter usually presents voltage source characteristics [32]. In fact, the detailed control schemes and topologies of IBR are even unavailable for utilities in practice. These facts make IBR difficult to be described with a model that is both generic and accurate.

To address the above challenges, the IBR side can be viewed as three "unavailable boxes" as shown in Fig. 2, where the subscripts 1, 2, and 0 correspond to the positive, negative, and zero sequence, respectively. The physical laws in sequence networks in Fig. 2 are summarized below.

In the positive sequence network, the Kirchhoff's voltage laws (KVLs) before and during the fault are as follows:

$$\begin{cases}\tilde{V}_{G1\_pre} = \tilde{I}_{G1\_pre}mZ_{1L} - \tilde{I}_{H1\_pre}((1-m)Z_{1L}+Z_{H1}) + \tilde{E}_{H1}\\ \tilde{V}_{G1} = \tilde{I}_{G1}mZ_{1L} - \tilde{I}_{H1}((1-m)Z_{1L}+Z_{H1}) + \tilde{E}_{H1}\end{cases} \tag{1}$$

where the variables with subscript "_pre" mean the quantities before the fault occurs.

The difference between the two rows of (1) is

$$\Delta\tilde{V}_{G1} = \Delta\tilde{I}_{G1}mZ_{1L} - \Delta\tilde{I}_{H1}[(1-m)Z_{1L}+Z_{H1}] \tag{2}$$

where $\Delta\tilde{X} = \tilde{X} - \tilde{X}_{\_pre}$, and $\tilde{X}$ corresponds to the voltage and-current phasors in Fig. 2.

Similarly, the Kirchhoff's current laws (KCLs) before and during the fault are as follows:

$$\begin{cases}\tilde{I}_{G1\_pre} + \tilde{I}_{H1\_pre} = 0\\ \tilde{I}_{G1} + \tilde{I}_{H1} - \tilde{I}_{F1} = 0.\end{cases} \tag{3}$$

The difference between the two rows of (3) is as follows:

$$\tilde{I}_{F1} = \Delta\tilde{I}_{G1} + \Delta\tilde{I}_{H1}. \tag{4}$$

Substitute (2) into (4) to eliminate $\Delta\tilde{I}_{H1}$. The expression of positive sequence fault current using local measurements is as follows:

$$\tilde{I}_{F1} = \frac{-\Delta\tilde{V}_{G1} + \Delta\tilde{I}_{G1}(Z_{1L}+Z_{H1})}{(1-m)Z_{1L}+Z_{H1}}. \tag{5}$$

In the negative sequence network, the KVL of the entire network and the KCL at the fault location during the fault are as follows:

$$\tilde{V}_{G2} = \tilde{I}_{G2}mZ_{2L} - \tilde{I}_{H2}((1-m)Z_{2L}+Z_{H2}) \tag{6}$$

$$\tilde{I}_{G2} + \tilde{I}_{H2} - \tilde{I}_{F2} = 0. \tag{7}$$

For typical power grids, the positive and negative sequence impedances of the protected line and remote end system are approximately equal [33], i.e. $Z_{1L} = Z_{2L}$ and $Z_{H1} = Z_{H2}$. Substitute (6) into (7)

$$\tilde{I}_{F2} = \frac{-\tilde{V}_{G2} + \tilde{I}_{G2}(Z_{1L}+Z_{H1})}{(1-m)Z_{1L}+Z_{H1}}. \tag{8}$$

In the zero sequence network, similarly as the derivation procedure in (6)–(8), the expression of zero sequence current is as follows:

$$\tilde{I}_{F0} = \frac{-\tilde{V}_{G0} + \tilde{I}_{G0}(Z_{0L}+Z_{H0})}{(1-m)Z_{0L}+Z_{H0}}. \tag{9}$$

With the IBR is modeled as "unavailable boxes" for relay element in power grid, the fault currents $\tilde{I}_{F1}$, $\tilde{I}_{F2}$, and $\tilde{I}_{F0}$ can still be expressed as functions of remote end source parameters and local terminal measurements.

Next, for various fault types, Section II-C to Section II-E derive the analytical expressions of fault distance m in detail as functions of line parameters and local terminal measurements before and during faults. The key idea is to combine equations within different sequence networks to eliminate unknown variables such as remote end voltage source parameters as well as the fault resistance, even with IBR unavailable box models.

C. Proposed Distance Protection for SPG Fault

The sequence network is connected with different topologies according to fault types [34]. The equivalent circuits of sequence networks for various fault types are shown in Fig. 3.

For single phase to ground (SPG) faults, A–G faults are taken as examples. The sequence network connection during A–G faults is shown in Fig. 3(a). Since the positive, negative and zero sequence networks during A–G faults are in series at the fault location, the KVLs are as follows:

$$\begin{cases}\tilde{V}_{G1} + \tilde{V}_{G2} + \tilde{V}_{G0} = (\tilde{I}_{G1} + \tilde{I}_{G2} + (k+1)\tilde{I}_{G0})mZ_{1L} + 3R_F\tilde{I}_{F1}\\ \tilde{V}_{G1} + \tilde{V}_{G2} + \tilde{V}_{G0} = (\tilde{I}_{G1} + \tilde{I}_{G2} + (k+1)\tilde{I}_{G0})mZ_{1L} + 3R_F\tilde{I}_{F2}\end{cases} \tag{10}$$

where $k = (Z_{0L} - Z_{1L})/Z_{1L}$. With $\tilde{V}_{GA} = \tilde{V}_{G1} + \tilde{V}_{G2} + \tilde{V}_{G0}$, substitute (5) and (8) into (10)

$$\tilde{V}_{GA} = (\tilde{I}_{GA} + k\tilde{I}_{G0})mZ_{1L} + 3R_F\frac{-\Delta\tilde{V}_{G1} + \Delta\tilde{I}_{G1}(Z_{H1}+Z_{1L})}{Z_{H1}+(1-m)Z_{1L}} \tag{11}$$

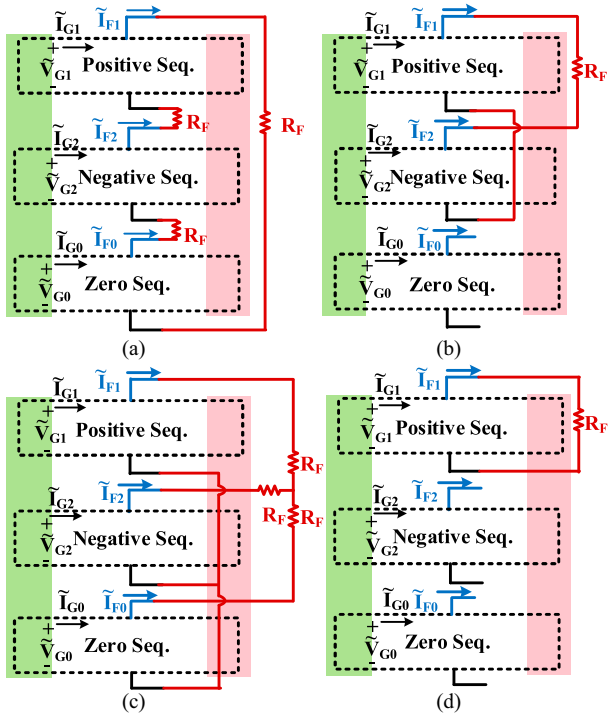

Fig. 3. Sequence network connections during various faults. (a) A–G faults. (b) B–C faults. (c) BC–G faults. (d) Three phase faults.

$$\tilde{V}_{GA}=(\tilde{I}_{GA}+k\tilde{I}_{G0})mZ_{1L}+3R_F\frac{-\tilde{V}_{G2}+\tilde{I}_{G2}(Z_{H1}+Z_{1L})}{Z_{H1}+(1-m)Z_{1L}}. \tag{12}$$

In (11) and (12), there are 4 real equations (real and imaginary parts of 2 complex equations) and 4 unknown variables (2 real unknown variables m and R_F, and 1 complex unknown variable Z_{H1}). From $(-\tilde{V}_{G2}+\tilde{I}_{G2}mZ_{1L})\times(11)-(-\Delta\tilde{V}_{G1}+\Delta\tilde{I}_{G1}mZ_{1L})\times(12)$, the remote source impedance Z_{H1} can be eliminated

$$\begin{aligned}&[(\tilde{I}_{GA}+k\tilde{I}_{G0})(\Delta\tilde{I}_{G1}-\tilde{I}_{G2})Z_{1L}{}^2]m^2-[\tilde{V}_{GA}(\Delta\tilde{I}_{G1}-\tilde{I}_{G2})\\&+(\Delta\tilde{V}_{G1}-\tilde{V}_{G2})(\tilde{I}_{GA}+k\tilde{I}_{G0})]Z_{1L}m+\tilde{V}_{GA}(\Delta\tilde{V}_{G1}-\tilde{V}_{G2})\\&+(-\Delta\tilde{I}_{G1}\tilde{V}_{G2}+\tilde{I}_{G2}\Delta\tilde{V}_{G1})3R_F=0.\end{aligned} \tag{13}$$

The real and imaginary parts of equation (13) can be rewritten as two real equations, with two real unknown variables m and R_F. By eliminating R_F, a quadratic equation of fault distance m can be obtained

$$am^2+bm+c=0 \tag{14}$$

$$\begin{cases}a=\text{imag}(k_3)\\b=\text{real}(k_1)\text{imag}(k_3)-\text{imag}(k_1)\text{real}(k_3)\\c=\text{real}(k_2)\text{imag}(k_3)-\text{imag}(k_2)\text{real}(k_3)\end{cases} \tag{15}$$

where the operators real$(\cdot)$ and imag$(\cdot)$ are the real and imaginary parts within brackets. The expression of variables k_1, k_2 and k_3 is depended on fault types. From (13), the expressions of those variables during A–G faults are shown in the following equation:

$$\begin{cases}k_1=\dfrac{-\tilde{V}_{GA}(\Delta\tilde{I}_{G1}-\tilde{I}_{G2})-(\Delta\tilde{V}_{G1}-\tilde{V}_{G2})(\tilde{I}_{GA}+k\tilde{I}_{G0})}{(\tilde{I}_{GA}+k\tilde{I}_{G0})(\Delta\tilde{I}_{G1}-\tilde{I}_{G2})Z_{1L}}\\k_2=\dfrac{\tilde{V}_{GA}(\Delta\tilde{V}_{G1}-\tilde{V}_{G2})}{(\tilde{I}_{GA}+k\tilde{I}_{G0})(\Delta\tilde{I}_{G1}-\tilde{I}_{G2})Z_{1L}{}^2}\\k_3=\dfrac{3(-\Delta\tilde{I}_{G1}\tilde{V}_{G2}+\tilde{I}_{G2}\Delta\tilde{V}_{G1})}{(\tilde{I}_{GA}+k\tilde{I}_{G0})(\Delta\tilde{I}_{G1}-\tilde{I}_{G2})Z_{1L}{}^2}.\end{cases} \tag{16}$$

The fault distance m can be solved analytically, as shown in (17). The negative root is neglected

$$m=\left(-b\pm\sqrt{b^2-4ac}\right)/(2a). \tag{17}$$

D. Proposed Distance Protection for PP Fault

This section derives the expression during phase to phase (PP) faults. Here B–C faults are taken as examples. The sequence network connection during B–C faults is shown in Fig. 3(b). Since the positive and negative sequence networks during B–C faults are in parallel at the fault location, the KVLs are

$$\tilde{V}_{G1}-\tilde{V}_{G2}=(\tilde{I}_{G1}-\tilde{I}_{G2})mZ_{1L}+R_F\frac{-\Delta\tilde{V}_{G1}+\Delta\tilde{I}_{G1}(Z_{H1}+Z_{1L})}{Z_{H1}+(1-m)Z_{1L}} \tag{18}$$

$$\tilde{V}_{G1}-\tilde{V}_{G2}=(\tilde{I}_{G1}-\tilde{I}_{G2})mZ_{1L}-R_F\frac{-\tilde{V}_{G2}+\tilde{I}_{G2}(Z_{H1}+Z_{1L})}{Z_{H1}+(1-m)Z_{1L}}. \tag{19}$$

Equations (18) and (19) include 4 real equations (2 complex equations) and 4 real unknown variables (real variables m and R_F, complex variable Z_{H1}). Eliminate Z_{H1} from (18) and (19)

$$\begin{aligned}&[(\tilde{I}_{G1}-\tilde{I}_{G2})(\Delta\tilde{I}_{G1}+\tilde{I}_{G2})Z_{1L}{}^2]m^2-[(\tilde{V}_{G1}-\tilde{V}_{G2})\\&(\Delta\tilde{I}_{G1}+\tilde{I}_{G2})+(\Delta\tilde{V}_{G1}+\tilde{V}_{G2})(\tilde{I}_{G1}-\tilde{I}_{G2})]Z_{1L}m+(\Delta\tilde{V}_{G1}\\&+\tilde{V}_{G2})(\tilde{V}_{G1}-\tilde{V}_{G2})+(-\Delta\tilde{I}_{G1}\tilde{V}_{G2}+\tilde{I}_{G2}\Delta\tilde{V}_{G1})R_F=0.\end{aligned} \tag{20}$$

Similarly, eliminate R_F in (20) to obtain a quadratic equation of m, with the standard format of (14) and (15). From (20), the expressions of k_1, k_2 and k_3 during B–C faults are derived as shown in the following equation:

$$\begin{cases}k_1=\dfrac{-(\tilde{V}_{G1}-\tilde{V}_{G2})(\Delta\tilde{I}_{G1}+\tilde{I}_{G2})-(\Delta\tilde{V}_{G1}+\tilde{V}_{G2})(\tilde{I}_{G1}-\tilde{I}_{G2})}{(\tilde{I}_{G1}-\tilde{I}_{G2})(\Delta\tilde{I}_{G1}+\tilde{I}_{G2})Z_{1L}}\\k_2=\dfrac{(\tilde{V}_{G1}-\tilde{V}_{G2})(\Delta\tilde{V}_{G1}+\tilde{V}_{G2})}{(\tilde{I}_{G1}-\tilde{I}_{G2})(\Delta\tilde{I}_{G1}+\tilde{I}_{G2})Z_{1L}{}^2}\\k_3=\dfrac{(-\Delta\tilde{I}_{G1}\tilde{V}_{G2}+\tilde{I}_{G2}\Delta\tilde{V}_{G1})}{(\tilde{I}_{G1}-\tilde{I}_{G2})(\Delta\tilde{I}_{G1}+\tilde{I}_{G2})Z_{1L}{}^2}.\end{cases} \tag{21}$$

E. Proposed Distance Relay for PPG Faults

This section derives the expression during phase to phase to ground (PPG) faults. Here BC–G faults are taken as examples.

The sequence network connection during BC–G faults is shown in Fig. 3(c). Since the three sequence networks during BC–G faults are in parallel at the fault location, the KVLs are as follows:

$$\begin{cases}\tilde{V}_{G1}-\tilde{V}_{G2}=(\tilde{I}_{G1}-\tilde{I}_{G2})mZ_{1L}+\tilde{I}_{F1}R_F-\tilde{I}_{F2}R_F\\ \tilde{V}_{G2}-\tilde{V}_{G0}=\tilde{I}_{G2}mZ_{1L}-\tilde{I}_{G0}mZ_{0L}+\tilde{I}_{F2}R_F-\tilde{I}_{F0}R_F.\end{cases} \tag{22}$$

Substitute (5) and (8) to the KCL at the fault point

$$\tilde{I}_{F0}=-\tilde{I}_{F1}-\tilde{I}_{F2}=\frac{(\Delta\tilde{V}_{G1}+\tilde{V}_{G2})-(\Delta\tilde{I}_{G1}+\tilde{I}_{G2})(Z_{H1}+Z_{1L})}{Z_{H1}+(1-m)Z_{1L}}. \tag{23}$$

Substitute (5), (8), and (23) into (22)

$$\begin{aligned}\tilde{V}_{G1}-\tilde{V}_{G2}=&(\tilde{I}_{G1}-\tilde{I}_{G2})mZ_{1L}+[-(\Delta\tilde{V}_{G1}-\tilde{V}_{G2})+\\&+(\Delta\tilde{I}_{G1}-\tilde{I}_{G2})(Z_{H1}+Z_{1L})]/[Z_{H1}+(1-m)Z_{1L}]R_F\end{aligned} \tag{24}$$

$$\begin{aligned}\tilde{V}_{G2}-\tilde{V}_{G0}=&(\tilde{I}_{G2}-\beta\tilde{I}_{G0})mZ_{1L}+[-(\Delta\tilde{V}_{G1}+2\tilde{V}_{G2})\\&+(\Delta\tilde{I}_{G1}+2\tilde{I}_{G2})(Z_{H1}+Z_{1L})]/[Z_{H1}+(1-m)Z_{1L}]R_F\end{aligned} \tag{25}$$

where β is defined as $\beta=Z_{0L}/Z_{1L}$.

Equations (24) and (25) include 4 real equations (2 complex equations) and 4 real unknown variables (2 real variables m, R_F, and 1 complex variables Z_{H1}). Eliminate Z_{H1} from (24) to (25)

$$\begin{aligned}&[(\Delta\tilde{I}_{G1}+2\tilde{I}_{G2})(\tilde{I}_{G1}-\tilde{I}_{G2})-(\Delta\tilde{I}_{G1}-\tilde{I}_{G2})(\tilde{I}_{G2}-\beta\tilde{I}_{G0})]Z_{1L}{}^2m^2\\&-[(\Delta\tilde{V}_{G1}+2\tilde{V}_{G2})(\tilde{I}_{G1}-\tilde{I}_{G2})+(\tilde{V}_{G1}-\tilde{V}_{G2})(\Delta\tilde{I}_{G1}+2\tilde{I}_{G2})\\&-(\Delta\tilde{V}_{G1}-\tilde{V}_{G2})(\tilde{I}_{G2}-\beta\tilde{I}_{G0})-(\tilde{V}_{G2}-\tilde{V}_{G0})(\Delta\tilde{I}_{G1}-\tilde{I}_{G2})]Z_{1L}m\\&+[(\Delta\tilde{V}_{G1}+2\tilde{V}_{G2})(\tilde{V}_{G1}-\tilde{V}_{G2})-(\Delta\tilde{V}_{G1}-\tilde{V}_{G2})(\tilde{V}_{G2}-\tilde{V}_{G0})]\\&-[(\Delta\tilde{V}_{G1}+2\tilde{V}_{G2})(\Delta\tilde{I}_{G1}-\tilde{I}_{G2})-(\Delta\tilde{V}_{G1}-\tilde{V}_{G2})(\Delta\tilde{I}_{G1}+2\tilde{I}_{G2})]R_F=0.\end{aligned} \tag{26}$$

Similarly, the quadratic equations of m can be derived by eliminating R_F, which can be rewritten in the standard format of (14) and (15). From (26), the expressions of k_1, k_2 and k_3 during BC–G faults are derived as shown in the following equation:

$$\begin{cases}k_1=\dfrac{-(\Delta\tilde{V}_{G1}+2\tilde{V}_{G2})(\tilde{I}_{G1}-\tilde{I}_{G2})-(\tilde{V}_{G1}-\tilde{V}_{G2})(\Delta\tilde{I}_{G1}+2\tilde{I}_{G2})}{[(\Delta\tilde{I}_{G1}+2\tilde{I}_{G2})(\tilde{I}_{G1}-\tilde{I}_{G2})-(\Delta\tilde{I}_{G1}-\tilde{I}_{G2})(\tilde{I}_{G2}-\beta\tilde{I}_{G0})]Z_{1L}}\\ \qquad+\dfrac{(\Delta\tilde{V}_{G1}-\tilde{V}_{G2})(\tilde{I}_{G2}-\beta\tilde{I}_0)+(\tilde{V}_{G2}-\tilde{V}_{G0})(\Delta\tilde{I}_{G1}-\tilde{I}_{G2})}{[(\Delta\tilde{I}_{G1}+2\tilde{I}_{G2})(\tilde{I}_{G1}-\tilde{I}_{G2})-(\Delta\tilde{I}_{G1}-\tilde{I}_{G2})(\tilde{I}_{G2}-\beta\tilde{I}_{G0})]Z_{1L}}\\ k_2=\dfrac{(\Delta\tilde{V}_{G1}+2\tilde{V}_{G2})(\tilde{V}_{G1}-\tilde{V}_{G2})-(\Delta\tilde{V}_{G1}-\tilde{V}_{G2})(\tilde{V}_{G2}-\tilde{V}_{G0})}{[(\Delta\tilde{I}_{G1}+2\tilde{I}_{G2})(\tilde{I}_{G1}-\tilde{I}_{G2})-(\Delta\tilde{I}_{G1}-\tilde{I}_{G2})(\tilde{I}_{G2}-\beta\tilde{I}_{G0})]Z_{1L}{}^2}\\ k_3=\dfrac{(\Delta\tilde{V}_{G1}-\tilde{V}_{G2})(\Delta\tilde{I}_{G1}+2\tilde{I}_{G2})-(\Delta\tilde{V}_{G1}+2\tilde{V}_{G2})(\Delta\tilde{I}_{G1}-\tilde{I}_{G2})}{[(\Delta\tilde{I}_{G1}+2\tilde{I}_{G2})(\tilde{I}_{G1}-\tilde{I}_{G2})-(\Delta\tilde{I}_{G1}-\tilde{I}_{G2})(\tilde{I}_{G2}-\beta\tilde{I}_{G0})]Z_{1L}{}^2}.\end{cases} \tag{27}$$

F. Distance Relay for Three Phase Faults

As shown in Fig. 3(d), the equivalent circuit during three phase faults only includes information in positive sequence. Since the proposed method requires more than one sequence network to eliminate unknown variables, the proposed method is not applicable to three phase faults. Fortunately, the fault resistances during three phase faults are typically small (<1 Ω as presented in [21], <5 Ω as presented in [35]). In this case, one can apply reactance method to deal with three phase faults, where the fault distance m can be calculated by $m=\text{imag}(\tilde{V}_{GA}/\tilde{I}_{GA})/\text{imag}(Z_{1L})$ [36]. Indeed, for extreme scenarios with high resistance three phase faults, further protection schemes should be studied in the future.

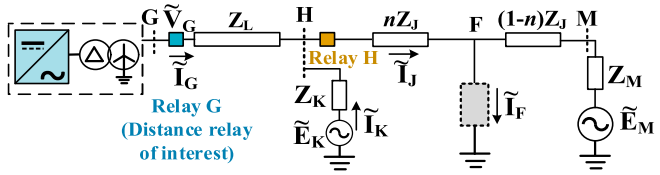

Fig. 4. System with external faults at line HM.

G. Illustration of Selectivity During Forward External Faults

The selectivity of the proposed method during forward external faults is illustrated in this section. Consider an example system with two branches (branch K and M) at the remote bus H, as shown in Fig. 4. The external faults in line HM occur at distance n from bus H. Here, A–G faults are taken as examples.

In the positive sequence network, the following equations can be obtained by the differences between equations before and during the fault

$$\begin{cases}\Delta\tilde{V}_{G1}=\Delta\tilde{I}_{G1}Z_{1L}+(\Delta\tilde{I}_{G1}+\Delta\tilde{I}_{K1}-\tilde{I}_{F1})(Z_{1J}+Z_{M1})+\tilde{I}_{F1}nZ_{1J}\\ \Delta\tilde{V}_{G1}-\Delta\tilde{I}_{G1}Z_{1L}+\Delta\tilde{I}_{K1}Z_{K1}=0.\end{cases} \tag{28}$$

Thus, the positive sequence fault current is as follows:

$$\tilde{I}_{F1}=\frac{(-\Delta\tilde{V}_{G1}+\Delta\tilde{I}_{G1}Z_{1L})(Z_{K1}+Z_{1J}+Z_{M1})/Z_{K1}+\Delta\tilde{I}_{G1}(Z_{1J}+Z_{M1})}{(1-n)Z_{1J}+Z_{M1}}. \tag{29}$$

In the negative sequence network, the circuit satisfies

$$\begin{cases}\tilde{V}_{G2}=\tilde{I}_{G2}Z_{1L}+(\tilde{I}_{G2}+\tilde{I}_{K2}-\tilde{I}_{F2})(Z_{1J}+Z_{M1})+\tilde{I}_{F2}nZ_{1J}\\ \tilde{V}_{G2}-\tilde{I}_{G2}Z_{1L}+\tilde{I}_{K2}Z_{K1}=0.\end{cases} \tag{30}$$

Similarly, the negative sequence fault current is as follows:

$$\tilde{I}_{F2}=\frac{(-\tilde{V}_{G2}+\tilde{I}_{G2}Z_{1L})(Z_{K1}+Z_{1J}+Z_{M1})/Z_{K1}+\tilde{I}_{G2}(Z_{1J}+Z_{M1})}{(1-n)Z_{1J}+Z_{M1}}. \tag{31}$$

Although here the fault is an external fault, the proposed method can still estimate the fault distance m using (13) after substituting the local measurements during this external fault. Note that here the value of m is not necessarily equal to the actual fault distance $1+n$, since the derivation in (13) assumes internal faults. Also, the fault resistance R_F^{ext} that satisfies (13) is typically not equal to the actual fault resistance R_F. Substitute the actual equations of fault current during external faults, i.e.

(29) and (31), into (13)

$$\frac{\tilde{I}_{F1}[(1-n)Z_{1J}+Z_{M1}]-\tilde{I}_{G2}(Z_{1J}+Z_{M1})}{(Z_{K1}+Z_{1J}+Z_{M1})/Z_{K1}}[\tilde{V}_{GA}-(\tilde{I}_{GA}+k\tilde{I}_{G0})mZ_{1L} -\Delta\tilde{I}_{G1}3R_F^{\text{ext}}]-\frac{\tilde{I}_{F1}[(1-n)Z_{1J}+Z_{M1}]-\Delta\tilde{I}_{G1}(Z_{1J}+Z_{M1})}{(Z_{K1}+Z_{1J}+Z_{M1})/Z_{K1}} \cdot[\tilde{V}_{GA}-(\tilde{I}_{GA}+k\tilde{I}_{G0})mZ_{1L}-\tilde{I}_{G2}3R_F^{\text{ext}}]=0. \tag{32}$$

From (32), the estimated distance m satisfies

$$\tilde{V}_{GA}-(\tilde{I}_{GA}+k\tilde{I}_{G0})mZ_{1L}-3\tilde{I}_{F1}R_F^{\text{ext}}\frac{(1-n)Z_{1J}+Z_{M1}}{Z_{1J}+Z_{M1}}=0. \tag{33}$$

On the other hand, the actual distance n should satisfy the following equation from KVL:

$$\tilde{V}_{GA}-(\tilde{I}_{GA}+k\tilde{I}_{G0})Z_{1L}-(\tilde{I}_{JA}+k\tilde{I}_{J0})nZ_{1J}-3\tilde{I}_{F1}R_F=0. \tag{34}$$

From (33) and (34), the relationship between estimated m and actual distance n is derived

$$\tilde{V}_{GA}-(\tilde{I}_{GA}+k\tilde{I}_{G0})mZ_{1L}-3[(1-n)Z_{1J}+Z_{M1}]/(Z_{1J}+Z_{M1}) \cdot[\tilde{V}_{GA}-(\tilde{I}_{GA}+k\tilde{I}_{G0})Z_{1L}-(\tilde{I}_{JA}+k\tilde{I}_{J0})nZ_{1J}]R_F^{\text{ext}}/R_F=0. \tag{35}$$

Eliminate the R_F and R_F^{ext} in (35) to obtain m

$$m=\frac{\text{imag}\left(\tilde{V}_{GA}\frac{Z_{1J}+Z_{M1}}{(1-n)Z_{1J}+Z_{M1}}\frac{1}{\tilde{V}_{FA}}\right)}{\text{imag}\left((\tilde{I}_{GA}+k\tilde{I}_{G0})Z_{1L}\frac{Z_{1J}+Z_{M1}}{(1-n)Z_{1J}+Z_{M1}}\frac{1}{\tilde{V}_{FA}}\right)} \tag{36}$$

where $\tilde{V}_{FA}=\tilde{V}_{GA}-(\tilde{I}_{GA}+k\tilde{I}_{G0})Z_{1L}-(\tilde{I}_{JA}+k\tilde{I}_{J0})nZ_{1J}$ is the voltage at the fault point F. For external faults in line HM (i.e. $0<n<1$), since Z_{1J} and Z_{M1} are both inductive in general, $(Z_{1J}+Z_{M1})/[(1-n)Z_{1J}+Z_{M1}]$ in (36) is close to a positive real number and will hardly contribute to the value of m. Define $p=m-1$, it can be expressed as

$$p\approx\text{imag}\left(\frac{(\tilde{I}_{JA}+k\tilde{I}_{J0})nZ_{1J}}{\tilde{V}_{FA}}\right)/\text{imag}\left(\frac{(\tilde{I}_{JA}+k\tilde{I}_{J0})Z_{1L}}{\tilde{V}_{FA}}\frac{\tilde{I}_{GA}+k\tilde{I}_{G0}}{\tilde{I}_{JA}+k\tilde{I}_{J0}}\right). \tag{37}$$

From (37), the fault point voltage satisfies $\tilde{V}_{FA}=\tilde{I}_{FA}R_F$, i.e., $\tilde{V}_{FA}$ and $\tilde{I}_{FA}$ have similar phase angles. Typically, compared to the IBR, the equivalent voltage source $\tilde{E}_K$ provides the majority of $\tilde{I}_J$ during external faults. One can assume that the phase angles of $\tilde{I}_{JA}+k\tilde{I}_{J0}$ and $\tilde{I}_{FA}$ are close to each other. With the line impedance nZ_{1J} and Z_{1L} are inductive, the phase angle of $(\tilde{I}_{JA}+k\tilde{I}_{J0})nZ_{1J}/\tilde{V}_{FA}$ and $(\tilde{I}_{JA}+k\tilde{I}_{J0})Z_{1L}/\tilde{V}_{FA}$ are both close to 90°. Thus, the numerator in (37) is a positive number.

Consider the real power in Fig. 4. During the external faults, the real power flowing into node H (from G) and the real power flowing out of node H (to F) should both be positive. Therefore, the phase angle of $(\tilde{I}_{GA}+k\tilde{I}_{G0})/(\tilde{I}_{JA}+k\tilde{I}_{J0})$ is between −90° and 90°. Combining these characteristics, the denominator term of (37) is also a positive value. Therefore, the solution satisfies $p>0$ (i.e. $m=1+p>1$) during external faults.

From (37), the difference between p and n mainly comes from the current injection from branch K. In this case, the estimated $m=1+p$ does not reflect the exact fault location $1+n$ for forward external faults. Nevertheless, the proposed distance relay can still correctly operate during the forward external faults. For Relay G in Fig. 4, since $m>1$ for forward external faults, these faults will fall outside of Zone-I; for Relay H in Fig. 4, these faults will fall within Zone-I. As a result, the selectivity of the proposed method is ensured, as it will not misoperate during forward external faults. Therefore, Zone-I and Zone-II of the distance relay can be designed accordingly.

H. Adaptability of Proposed Method to Various Sources

In fact, the impact of IBR on line distance protection has two aspects. First, the IBR side demonstrates a weak-infeed feature, i.e., the limited fault current at the IBR side is much less than that at the power grid side. As a result, the weak-infeed feature will magnify the impact of fault resistance on the distance protection. This phenomenon also exists for weak-infeed lines terminated by only SGs. Second, due to complicated response features of IBR control during faults, the equivalent source voltage and impedance of IBR varies greatly during faults, causing further challenges for mitigating the impact of fault resistance on the distance protection. This phenomenon does not exist for lines terminated by only SGs.

The principle of the proposed method is to utilize independent equations for multiple sequence networks, to eliminate the effect of remote infeed current and fault resistance, thereby improving reliability of distance relay. It is worth noting that, if the local bus only connects SGs (no IBRs) and the positive/negative sequence source impedances of SGs are the same (i.e., $\Delta\tilde{V}_{G1}/\Delta\tilde{I}_{G1}=\tilde{V}_{G2}/\tilde{I}_{G2}$), the effectiveness of proposed method might be limited. One can observe that the impedances of the line and the remote end source for the positive sequence are identical to those for the negative sequence. For A–G faults, $\tilde{I}_{F1}=\tilde{I}_{F2}$, i.e. $\Delta\tilde{I}_{G1}+\Delta\tilde{I}_{H1}=\tilde{I}_{G2}+\tilde{I}_{H2}$. With the same positive/negative impedances, the fault current distributions are identical for positive and negative sequences, i.e. $\Delta\tilde{I}_{G1}=\tilde{I}_{G2}$ and thus $\Delta\tilde{V}_{G1}=\tilde{V}_{G2}$. This means equations (11) and (12) are the same and not independent. As a result, the coefficients k_1, k_2, and k_3 in (16) are all are equal to zero so that m has infinite number of solutions. For B–C faults, $\tilde{I}_{F1}=-\tilde{I}_{F2}$, i.e. $\Delta\tilde{I}_{G1}+\Delta\tilde{I}_{H1}=-\tilde{I}_{G2}-\tilde{I}_{H2}$. Similarly, the fault current distributions are identical for positive and negative sequences, i.e. v and thus $\Delta\tilde{V}_{G1}=-\tilde{V}_{G2}$. This means equations (18) and (19) are the same and not independent. As a result, the coefficients k_1, k_2, and k_3 in (21) are all are equal to zero so that m has infinite number of solutions. For BC–G faults, the proposed method is not affected by the above situation.

Fortunately, the complicated characteristics of IBR during faults (determined by complex control schemes, nonideal phase-locked loops, power electronic switches, etc.) make the features of positive and negative sequence network not strictly identical. This guarantees that the equations for positive and negative sequence networks are independent and enables the proposed

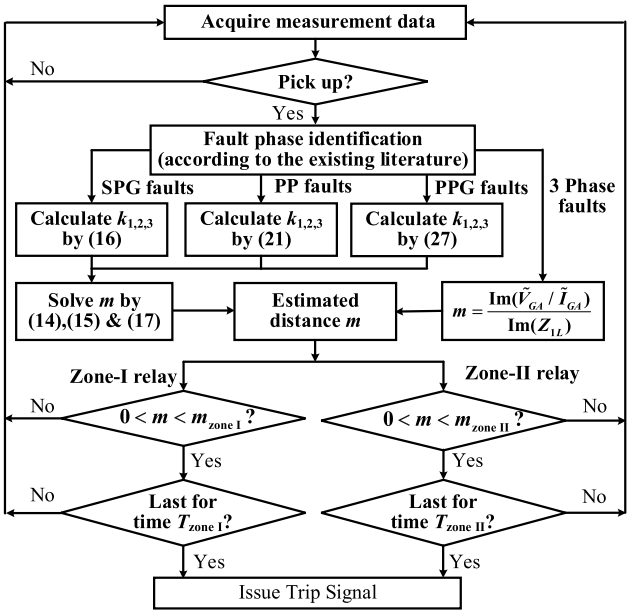

Fig. 5. Flow diagram of the proposed method.

method. Even if the local bus is connected to both SGs and IBRs, positive and negative sequence networks are also not strictly identical so that the proposed method is still effective.

I. The Structure of Proposed Protection

This section summarizes the implementation process of the proposed distance protection. When the fault occurs, the abnormal voltage is usually adopted as the pick-up criterion [23]. Fault phase identification [34], [37], [38], [39], [40], [41] is also a hot research topic, especially for lines terminated by IBRs. By extracting feature components [34], [37], [38] and improving phase selection criteria [39], [40], [41], these methods improve the speed and accuracy of phase selection procedure. In this article, the phase selection procedure adopts existing literature [40] as an example. After that, the coefficients k_1, k_2, and k_3 are calculated by (16), (21), and (27) according to fault types. Next, the fault distance m is calculated by (14), (15), and (17) during asymmetric faults. For 3 phase faults, the m is estimated by reactance method [35].

Next, the estimated m is compared to settings of different zones for trip decision. Zone-I covers the majority of the line under protection, (e.g. $m_{\mathrm{zoneI}} = 80\%$ of the line, with a short trip delay of $T_{\mathrm{zoneI}} = 2$ cycles). Zone-II covers the entire length of the line with slight overreach characteristics (e.g. $m_{\mathrm{zoneII}} = 120\%$ of the line, with a longer trip delay of $T_{\mathrm{zoneII}} = 10$ cycles), which coordinates with the Zone-I relay of the next line, to ensure selectivity during external faults [41]. In practice, the above settings m_{zoneI}, T_{zoneI}, m_{zoneII}, and T_{zoneII} can also be adjusted according to the preference of the users. The flow diagram of proposed distance relay is summarized in Fig. 5.

III. Simulation

An example test system is built in MATLAB/Simulink, as shown in Fig. 6. The system is a 50 Hz 110 KV system, with a

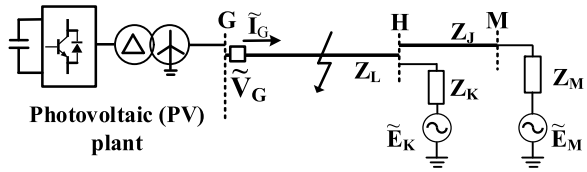

Fig. 6. Example test system for simulation.

TABLE I
Line Parameters for Simulation

Line	Pos. Seq.	Value	Zero Seq.	Value
Line GH	R_{1L}	0.10 Ω/km	R_{0L}	0.42 Ω/km
	L_{1L}	1.61 mH/km	L_{0L}	3.84 mH/km
	C_{1L}	8.1 nF/km	C_{0L}	5.2 nF/km
Line HM	R_{1J}	0.07 Ω/km	R_{0J}	0.31 Ω/km
	L_{1J}	1.54 mH/km	L_{0J}	3.59 mH/km
	C_{1L}	9.5 nF/km	C_{0L}	6.9 nF/km

30 MW photovoltaic plant connected to the Bus G. The step-up transformer is Δ-YN connected with neutral point grounded. The length of line GH and HM are 100 km and 80 km, respectively. The line parameters are shown in Table I.

The distance relay of interest is the relay at terminal G. The sampling frequency of three phase voltage and current measurement is 10 kHz. Phasors are calculated according to IEC-60255. The settings of the proposed distance relay are: $m_{\mathrm{zoneI}} = 80\%$, $T_{\mathrm{zoneI}} = 2$ cycles, $m_{\mathrm{zoneII}} = 120\%$, $T_{\mathrm{zoneII}} = 10$ cycles.

A. Relay Performances During Various Fault Types

Recently, various grid codes require IBR to inject negative sequence current when the system is unbalanced. In this section, the inverter adopts active–reactive power control scheme, with the ride-through mode that injects negative sequence current based on negative sequence voltage, as described in IEEE Std 2800-2022 [17].

Six case groups are presented, including A–G faults (group 1&2), B–C faults (group 3&4) and BC–G faults (group 5&6). All faults occur at 0.1 s. Groups 1, 3 and 5 are 1 Ω low resistance faults, while Groups 2, 4, and 6 are high resistance faults. For SPG faults, the maximum fault resistances considered in the existing literature could vary from 30 to 100 Ω [15], [27], [43], [44]. For PP or PPG faults, the maximum fault resistances could vary from 10 to 20 Ω [1], [5], [45]. Therefore, this article considers the maximum fault resistance of 75 Ω for A–G faults, and 15 Ω for B–C and BC–G faults. Each group includes Zone-I faults at 10%, 50%, and 75% of the protected line, Zone-II faults at 90% and 110% of the protected line, and fault at 150% (outside of trip zone) of the protected line.

The performances of the proposed distance protection during faults in Groups 1 to 6 are shown in Fig. 7. When internal faults at 10%, 50%, and 75% occur, the calculated values of m become quite close to the actual fault locations during steady state, regardless of low or high fault resistances. All above 3 Zone-I faults are correctly tripped by Zone-I relay. Meanwhile, Zone-II faults at 90% of the line are correctly tripped by Zone-II relay.

For external faults at 110% and 150%, the calculated m could vary for various fault types and fault resistances during steady

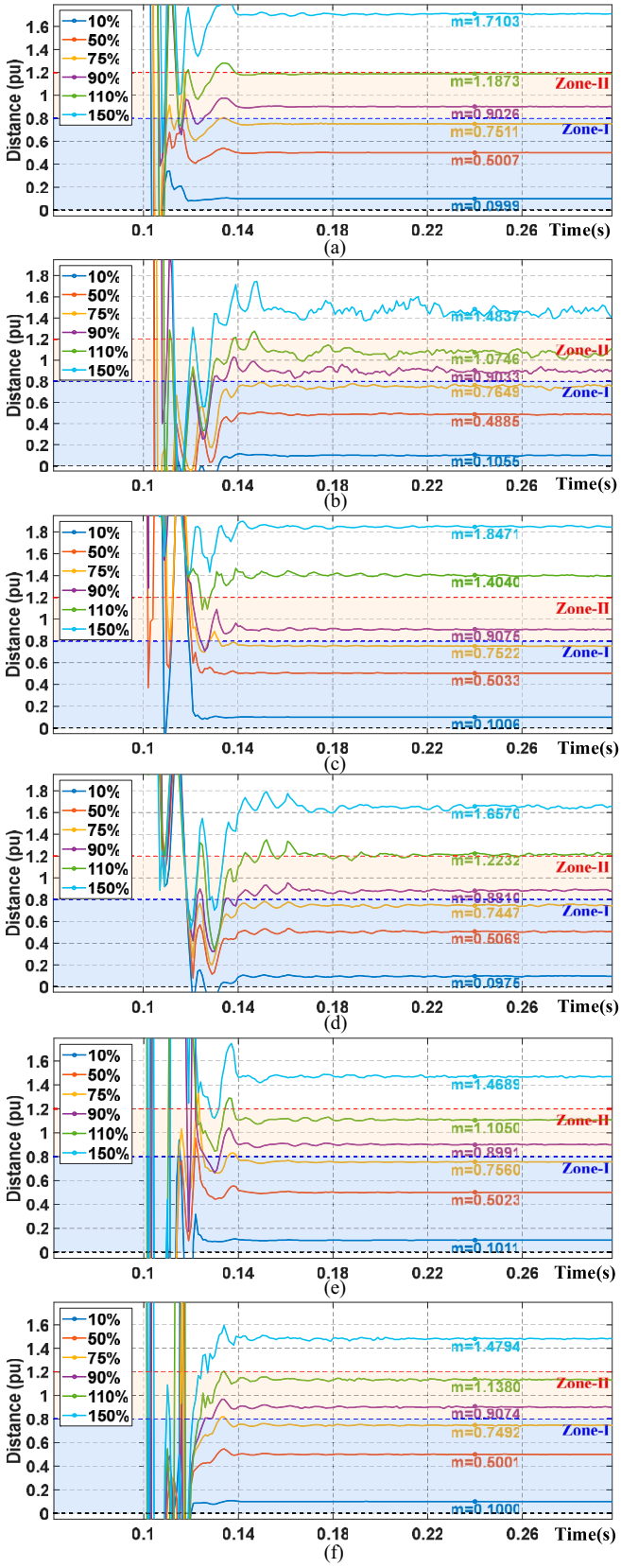

Fig. 7. Proposed relay performances, negative sequence current injection IBR control: (a) group 1, 1 Ω A–G faults; (b) group 2, 75 Ω A–G faults; (c) group 3, 1 Ω B–C faults; (d) group 4, 15 Ω B–C faults; (e) group 5, 1 Ω BC–G faults; and (f) group 6, 15 Ω BC–G faults.

state. This is because different fault scenarios could cause different infeed currents from branch K. For example, calculated values of m falls inside Zone-II during 110% A–G and BC–G faults, but falls outside Zone-II during 110% B–C fault. Nevertheless, these external faults still stay outside of Zone-I of the protected line. Since these external faults will be instantaneously tripped by the relay at line HM, it ensures that the relay of the protected line will correctly refuse to operate during these external faults.

During various faults, the calculated values of m will oscillate before reaching steady state. Most oscillations occur within first 2 cycles after the occurrence of the fault. In fact, the oscillations could also be observed during calculation of apparent impedances of legacy distance protection for lines terminated by SGs. The Zone-I trip delay T_{zoneI} manages to avoid the impacts of the oscillations on the protection reliability, and also meets the fault clearing requirements of ac lines [16].

B. Impact of Control Strategies

Unlike IEEE Std 2800-2022, some grid codes do not specify the negative sequence characteristics under unbalanced conditions [46]. In this section, control strategy suppressing negative sequence currents [5], [16] is adopted as examples to verify the compatibility of the proposed method. Due to space limitation, three groups of high resistance faults are taken as examples, which include 75Ω A–G faults (Group 7), 15Ω B–C faults (Group 8) and 15Ω BC–G faults (Group 9). They correspond to Groups 2, 4, and 6 in Section III-A. The performances of the proposed method are shown in Fig. 8.

When internal faults occur, the calculated values of m approach the actual fault distance in 2 cycles. The faults at 10%, 50%, and 75% of the protected line are tripped by Zone-I relay correctly, and faults at 90% of the line are protected by Zone-II relay. When external faults occur, the calculated values of m keep larger than 1. Thus, these external faults will be instantaneously tripped by the relay at line HM. The results in Section III-A and III-B prove that the proposed method is compatible with both negative sequence current injection and negative sequence current suppression control schemes.

C. Impact of Branches at Local Bus

In practical power grid, it is possible that the local bus G includes both the IBR and other branches. In this section, an equivalent source $\tilde{E}_N$ with internal impedance Z_N is connected to bus G via a 40 km line NG, as shown in Fig. 9. The control strategy of IBR is injecting negative sequence current during faults, which is the same as that in Section III-A. Similar as Group 2, 4, and 6 in Section III-A, three groups of high resistance faults are presented, including 75 Ω A–G faults (Group 10), 15 Ω B–C faults (Group 11) and 15 Ω BC–G faults (Group 12). The performances of the proposed method are shown in Fig. 10.

With a branch connected to bus G, the calculated m also approaches the actual fault distance when internal faults occur.

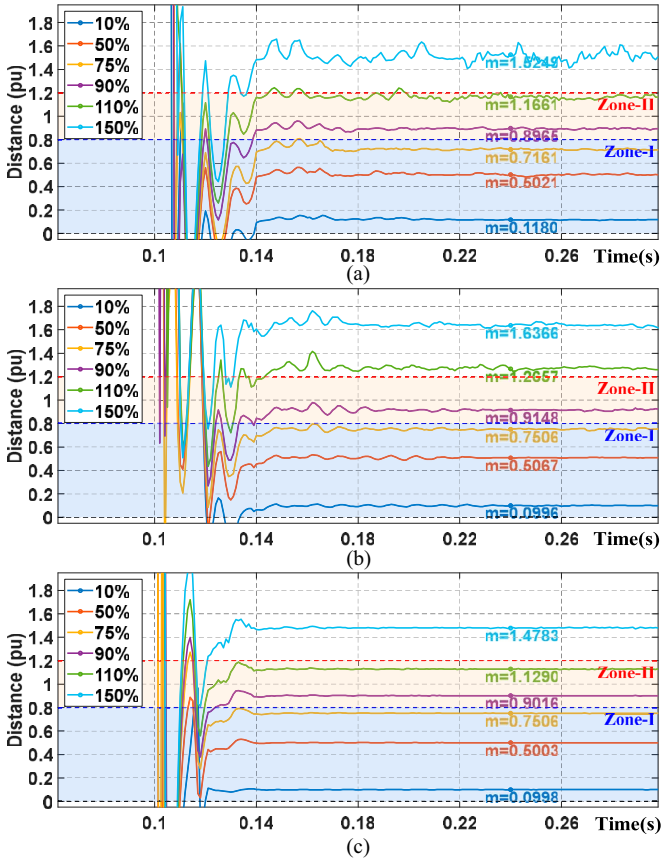

Fig. 8. Proposed relay performances, negative sequence current suppression IBR control: (a) group 7, 75 Ω A–G faults; (b) group 8, 15 Ω B–C faults; and (c) group 9, 15 Ω BC–G faults.

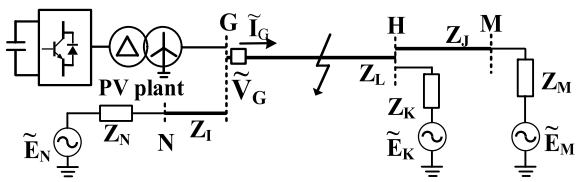

Fig. 9. Example test system for simulation with an extra branch.

The faults at 10%, 50% and 75% of the protected line are tripped by Zone-I relay correctly, and faults at 90% of the line are protected by Zone-II relay. For the forward external faults, the calculated values of m stay outside of Zone-I of the protected line and they will be instantaneously tripped by the relay at the line HM. The proposed method can work properly with additional branch at the local bus.

D. Impact of Winding Connection of IBR Transformer

Although Fig. 6 adopts Δ-YN connected transformer with neutral point grounded, the derivation of the proposed method simply treats the IBR as an unavailable box and does not have specific assumption on the transformer winding connection.

To verify compatibility of the proposed method with various winding connections, the transformer in Fig. 6 is replaced by y-YN winding with neutral point grounded at the high voltage side [47]. Here, the control strategy of IBR is also injecting negative

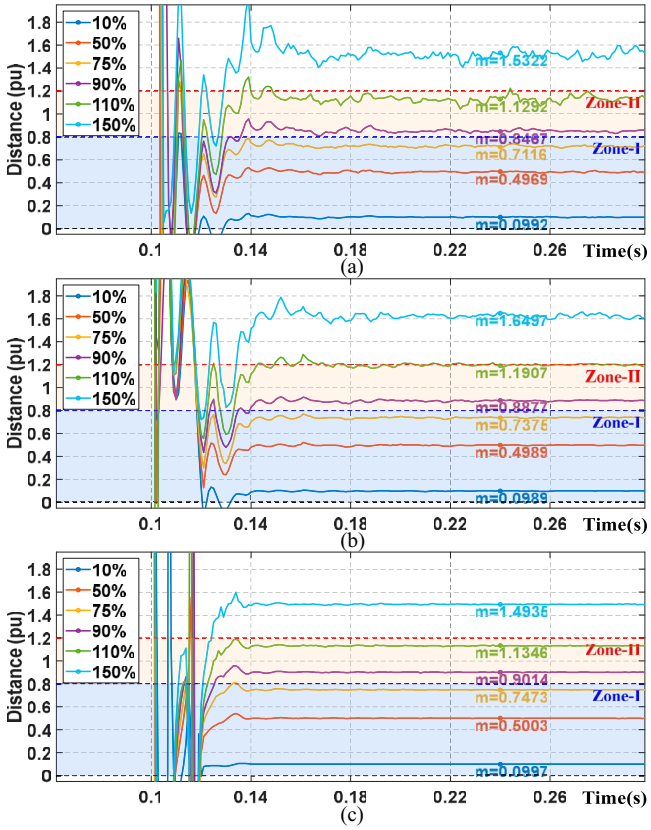

Fig. 10. Proposed relay performances, negative sequence current injection IBR control, branches at the local bus: (a) group 10, 75 Ω A–G faults; (b) group 11, 15 Ω B–C faults; and (c) group 12, 15 Ω BC–G faults.

sequence current during faults, as described in Section III-A. Similar as Group 2, 4, and 6, three groups of high resistance faults including 75 Ω A–G faults (Group 13), 15 Ω B–C faults (Group 14) and 15 Ω BC–G faults (Group 15) are presented. The performances of the proposed method are shown in Fig. 11.

For the IBR transformer using y-YN connection, the faults at 10%, 50%, and 75% of the protected line are correctly tripped by Zone-I relay, and the faults at 90% of the line are correctly tripped by Zone-II relay. During external faults, the proposed relay at terminal G will correctly refuse to operate, while the relay of line HM at terminal H will correctly trip these faults. The proposed method is compatible with various transformer winding connections.

IV. Comparison to Existing Methods

A. Legacy Method

The legacy distance protection adopts quadrilateral impedance characteristics to show robustness against fault resistances. Here, the performances of the legacy method are demonstrated with Group 4 (15Ω B–C faults) and Group 6 (15Ω BC–G faults). The settings of the legacy method are determined by the principle in [42]. The trajectory of the apparent impedance "seen" by the relay is plotted in an R-X complex plane, as shown in Fig. 12. The time stamps of the trajectory with faults at 10% are marked in the figure as examples.

During B–C faults at 10%, 50%, 75%, and 90% of the line and BC–G faults at 10% of the line, the apparent impedances

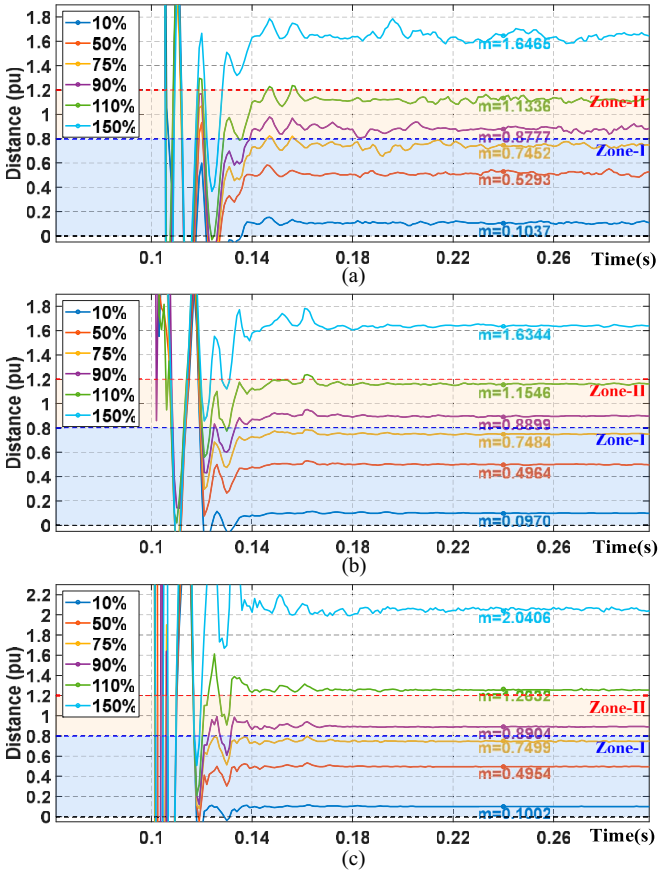

Fig. 11. Proposed relay performances, negative sequence current injection IBR control, y-YN transformer: (a) group 13, 75 Ω A–G faults; (b) group 14, 15 Ω B–C faults; and (c) group 15, 15 Ω BC–G faults.

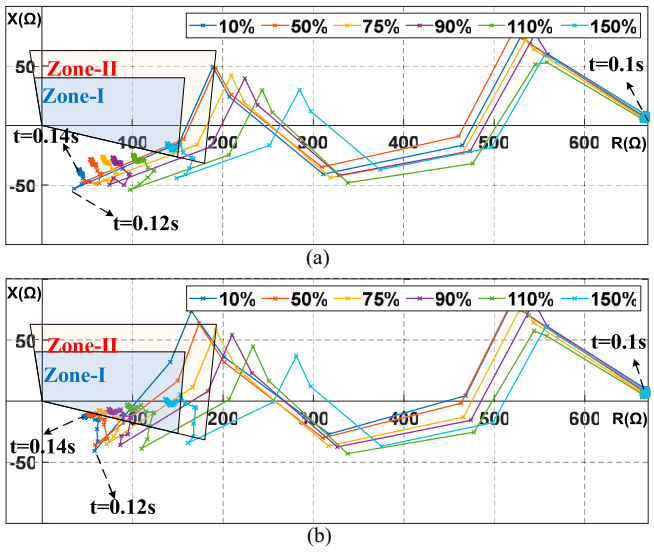

Fig. 12. Relay performances of legacy relay. (a) Group 4. (b) Group 6.

fall outside the tripping Zone-I, i.e., the relay cannot dependably trip these faults. During 150% B–C faults and 110%, 150% BC–G faults, the apparent impedances fall inside the tripping Zone-I, i.e., the relay cannot securely ignore those external faults, because the imaginary parts of the apparent impedance become negative with impact of IBR. These results prove that

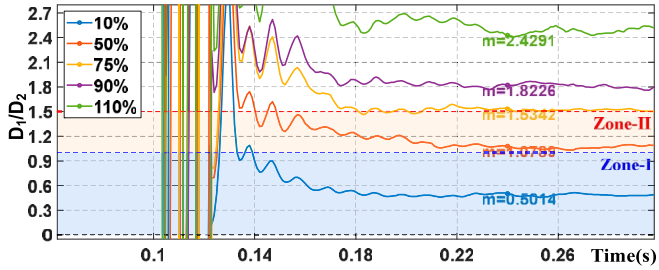

Fig. 13. Relay performances of existing improved method 1, group 4.

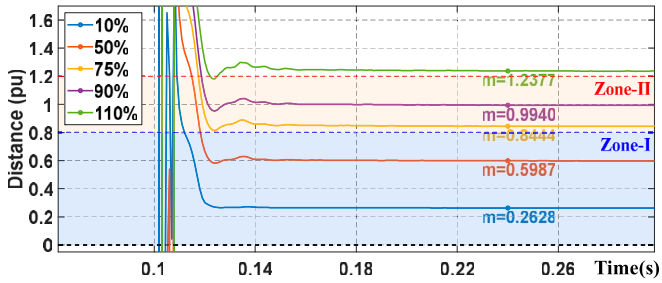

Fig. 14. Relay performances of existing improved method 2, group 6.

the legacy relay cannot dependably and securely operate for lines terminated by IBRs.

B. Existing Improved Method 1

The existing improved method 1 [21] calculates the value of D_1/D_2, where D_1 is a function of apparent impedance, and D_2 is a function of line impedance. The values of D_1 and D_2 are also functions of the phase angles of faulted path currents. Specifically, for PP faults, the method assumes that the phase angle of the faulted path current is close to that of negative sequence currents at the local end [19]. The effectiveness of this assumption depends on the availability of SGs at the IBR side.

The relay performances of the existing improved method 1 are demonstrated with Group 4 (15Ω B–C faults) in Section III-A as an example. The results are shown in Fig. 13. The existing improved method 1 fails to trip internal faults at 50%, 75%, and 90% of the line. The results show that the existing improved method 1 could encounter challenges during PP faults.

C. Existing Improved Method 2

The existing improved method 2 in [23] applies the negative sequence model to estimate fault location. Compared to [22] with the assumption of no negative sequence current injection for IBRs, existing improved method 2 adopts a compensation process for IBRs with negative sequence current injection. During derivation, the method assumes that the negative sequence voltages at the IBR and at the fault location are similar, which could cause compensation errors.

Next, the performances of the existing improved method 2 [23] are demonstrated with Group 6 (15Ω BC–G faults) in Section III-A as an example. The results are shown in Fig. 14. Due to compensation error of negative sequence currents, the estimated fault distance is slightly larger than its actual values. As a result, the fault at 75% of the protected line in Zone-I will be seen

TABLE II
COMPARISON BETWEEN PROPOSED DISTANCE PROTECTION AND EXISTING METHODS

Methods	No Need for Communication From Remote End?	Compatible With Various IBR Controls and Grid Codes?	Independent of Specific Assumptions/Requirements?
Ref. [18]	Remote end voltage	Yes	Requirement: time domain measurements with high sampling rate (> tens of kHz)
Ref. [19]	Remote end impedance	Yes	Requirement: IBR parameters to model IBR equivalent impedance
Ref. [20]	Remote end impedance	Yes	Yes
Ref. [21]	Yes	No	Assumption: faulted path currents and local current have similar phase angles
Ref. [22]	Yes	No	Assumption: no negative sequence current for IBRs
Ref. [23]	Yes	No	Assumption: similar negative sequence voltages at IBR and at fault location
Ref. [24]	Yes	No	Requirement: adjusting IBR control strategies according to various fault types
Ref. [25]	Yes	No	Requirement: adjusting IBR control strategies to inject specific reactive current
Ref. [26]	Yes	No	Requirement: adjusting IBR control strategies to inject specific harmonic current
Proposed	Yes	Yes	Yes

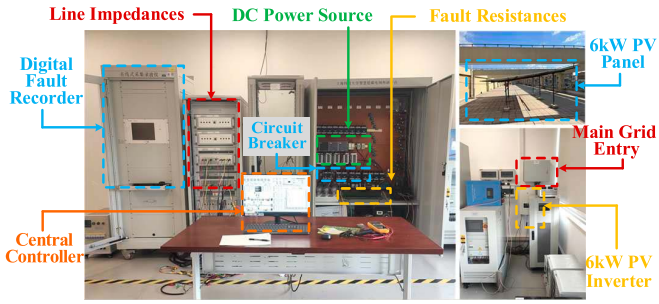

Fig. 15. Hardware experimental platform.

by Zone-II, limiting the operating speed of the relay during internal faults.

D. Summary of Existing Improved Methods

Besides the above two improved methods, there are many other improved methods with various features, such as requirement of additional measurement [18] or communication [19], [20] from the remote end, and requirement of certain grid codes with specific assumptions [21], [22], [23] or certain IBR control schemes during faults [24], [25], [26]. The comparisons of existing improved methods are summarized in Table II. One can observe that the proposed method works with present phasor measurements, does not require communication, and is compatible with various IBR control schemes and grid codes.

V. HARDWARE EXPERIMENTS

The experimental platform is a grid-connected photovoltaic system, as shown in Fig. 15. The system includes

1) A 6 kW PV panel connected to a 6 kW PV inverter.
2) Impedance boxes to represent line impedances.
3) Circuit breakers powered by dc sources to enable line fault.
4) Ceramic resistances as fault resistances.
5) The 220 V main grid.

During normal operation, the PV inverter is connected to the main grid via the line impedances. The overall line impedances are $Z_{1L} = j7.35\ \Omega$ and $Z_{0L} = j19.13\ \Omega$. The line impedances are

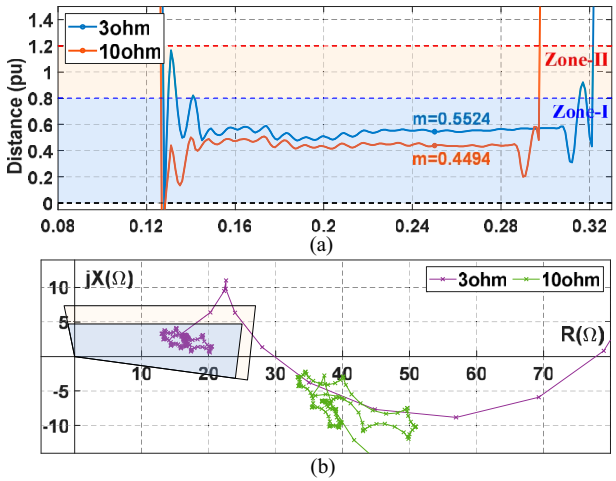

Fig. 16. Relay performances with hardware experiments. (a) Proposed method. (b) Legacy method.

divided into two sections and the fault resistance is connected to the node between two sections. The digital fault recorder (DFR) is deployed to measure local voltage and current signals before and during the fault, with the sampling rate of 5 kHz. The recorded data are stored in COMTRADE files.

Next, two fault events are considered, including a 3 Ω A–G fault and a 10 Ω A–G fault at 52% of the line. The performances of the legacy method with quadrilateral impedance characteristics and the proposed method are presented for comparison. The settings of the proposed relay and legacy relay are consistent with those in Sections III and IV-A. The results are shown in Fig. 16. By estimating fault distance, the proposed method can trip correctly during both fault events, but the legacy method fails to trip during the 10 Ω fault. The result verifies the effectiveness of the proposed method.

VI. FIELD DATA EXPERIMENTS

The proposed method is also verified via field data. The C–G fault occurs on a 220 kV, 48 km transmission line, at 23% of the line. The line connects a PV plant to main grid. The overall line impedances are $Z_{1L} = 2.31 + j9.78\ \Omega$ and $Z_{0L} = 4.29 + j26.73\ \Omega$.

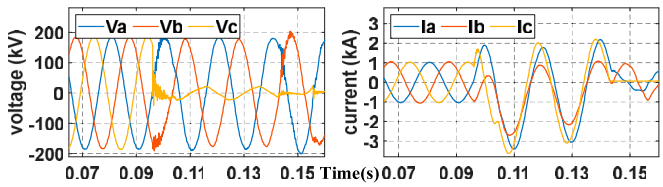

Fig. 17. Voltage and current waveforms at PV side, field data.

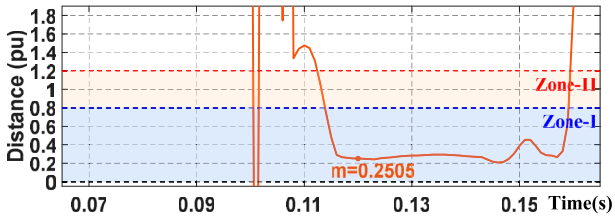

Fig. 18. Proposed relay performances, field data.

The voltage and current waveforms before and during the fault are stored in COMTRADE files with 10 kHz sampling rate, as shown in Fig. 17. The fault occurs at approximately 0.0961 s. The performance of the proposed method is shown in Fig. 18. The calculated m stays at around 0.25 during the fault, supporting the effectiveness of the proposed method in practice.

VII. Conclusion

The increasing penetration of IBRs brings a series of challenges to the protection of transmission lines. This article proposes an improved distance protection for lines connected to IBRs, without additional measurement from the remote end. Utilizing the information of multiple sequence networks, the proposed protection analytically estimates the fault distance in real time. Compared to the existing methods, the proposed method greatly mitigates the effect of fault resistances and remote end infeed currents, independent of the IBR control schemes. As a result, the proposed distance relay improves the protection dependability and security for the lines terminated by IBRs. Simulation, hardware experiments and field data experiments support the effectiveness of the proposed distance relay with various inverter control schemes and grid codes.

Acknowledgment

The grant support is greatly appreciated.

References

[1] A. Hooshyar, M. A. Azzouz, and E. F. El-Saadany, "Distance protection of lines emanating from full-scale converter-interfaced renewable energy power plants—Part I: Problem Statement," *IEEE Trans. Power Del.*, vol. 30, no. 4, pp. 1770–1780, Aug. 2015.

[2] R. Chowdhury and N. Fischer, "Transmission line protection for systems with inverter-based resources Part I: Problems," *IEEE Trans. Power Del.*, vol. 36, no. 4, pp. 2416–2425, Aug. 2021.

[3] L. Huang, C. Wu, D. Zhou, and F. Blaabjerg, "A power-angle-based adaptive overcurrent protection scheme for grid-forming inverter under large grid disturbances," *IEEE Trans. Ind. Electron.*, vol. 70, no. 6, pp. 5927–5936, Jun. 2023.

[4] T. Zhang et al., "Impact of control interaction of wind farm with MMC-HVDC transmission system on distance protection adaptability under symmetric fault," *Prot. Control Mod. Power Syst.*, vol. 10, no. 2, pp. 83–101, Mar. 2025.

[5] Y. Fang et al., "Impact of inverter-interfaced renewable energy generators on distance protection and an improved scheme," *IEEE Trans. Ind. Electron.*, vol. 66, no. 9, pp. 7078–7088, Sep. 2019.

[6] B. Wang, J. Geng, and X. Dong, "High-impedance fault detection based on nonlinear voltage–current characteristic profile identification," *IEEE Trans. Smart Grid*, vol. 9, no. 4, pp. 3783–3791, Jul. 2018.

[7] L. Tang et al., "A new differential protection of transmission line based on equivalent travelling wave," *IEEE Trans. Power Del.*, vol. 32, no. 3, pp. 1359–1369, Jun. 2017.

[8] M. Tajdinian and H. Samet, "Divergence distance based index for discriminating inrush and internal fault currents in power transformers," *IEEE Trans. Ind. Electron.*, vol. 69, no. 5, pp. 5287–5294, May 2022.

[9] L. Zheng, K. Jia, T. Bi, Y. Fang, and Z. Yang, "Cosine similarity based line protection for large-scale wind farms," *IEEE Trans. Ind. Electron.*, vol. 68, no. 7, pp. 5990–5999, Jul. 2021.

[10] A. P. Meliopoulos et al., "Dynamic state estimation-based protection: Status and promise," *IEEE Trans. Power Del.*, vol. 32, no. 1, pp. 320–330, Feb. 2017.

[11] Y. Liu et al., "Dynamic state estimation for power system control and protection," *IEEE Trans. Power Syst.*, vol. 36, no. 6, pp. 5909–5921, Nov. 2021.

[12] Y. Liang, Y. Ren, and Z. Zhang, "Pilot protection based on two-dimensional space projection of dual differential currents for lines connecting MMC–HVDC stations," *IEEE Trans. Ind. Electron.*, vol. 70, no. 5, pp. 4356–4368, May 2023.

[13] K. Jia et al., "Influence of inverter-interfaced renewable energy generators on directional relay and an improved scheme," *IEEE Trans. Power Electron.*, vol. 34, no. 12, pp. 11843–11855, Dec. 2019.

[14] R. Chowdhury and N. Fischer, "Transmission line protection for systems with inverter-based resources Part I: Problems," *IEEE Trans. Power Del.*, vol. 36, no. 4, pp. 2416–2425, Aug. 2021.

[15] A. Banaiemoqadam et al., "Impact of inverter-based resources on different implementation methods for distance relays—Part I: Phase comparators," *IEEE Trans. Power Del.*, vol. 38, no. 6, pp. 4090–4102, Dec. 2023.

[16] J. Jia, G. Yang, A. H. Nielsen, and P. Rønne-Hansen, "Impact of VSC control strategies and incorporation of synchronous condensers on distance protection under unbalanced faults," *IEEE Trans. Ind. Electron.*, vol. 66, no. 2, pp. 1108–1118, Feb. 2019.

[17] *IEEE Standard for Interconnection and Interoperability of Inverter-Based Resources (IBRs) Interconnecting with Associated Transmission Electric Power Systems*, *IEEE Std 2800-2022*, Apr. 2022.

[18] P. Adhikari, S. Brahma, and P. H. Gadde, "Source-agnostic time-domain distance relay," *IEEE Trans. Power Del.*, vol. 37, no. 5, pp. 3620–3629, Oct. 2022.

[19] P. Mishra, A. K. Pradhan, and P. Bajpai, "Adaptive distance relaying for distribution lines connecting inverter-interfaced solar PV plant," in *IEEE Trans. Ind. Electron.*, vol. 68, no. 3, pp. 2300–2309, Mar. 2021.

[20] N. George, O. D. Naidu, and A. K. Pradhan, "Distance protection for lines connecting converter interfaced renewable power plants: Adaptive to grid-end structural changes," *IEEE Trans. Power Del.*, vol. 38, no. 3, pp. 2011–2021, Jun. 2023.

[21] S. Paladhi, J. R. Kurre, and A. K. Pradhan, "Source-independent zone-1 protection for converter-dominated power networks," *IEEE Trans. Power Del.*, vol. 39, no. 1, pp. 341–351, Feb. 2024.

[22] Y. Liang, W. Li, and Y. Huo, "Zone I distance relaying scheme of lines connected to MMC-HVDC stations during asymmetrical faults: Problems, challenges, and solutions," *IEEE Trans. Power Del.*, vol. 36, no. 5, pp. 2929–2941, Oct. 2021.

[23] C. Chao et al., "Adaptive distance protection based on the analytical model of additional impedance for inverter-interfaced renewable power plants during asymmetrical faults" *IEEE Trans. Power Del.*, vol. 37, no. 5, pp. 3823–3834, Oct. 2022.

[24] A. Banaiemoqadam, A. Hooshyar, and M. A. Azzouz, "A comprehensive dual current control scheme for inverter-based resources to enable correct operation of protective relays," *IEEE Trans. Power Del.*, vol. 36, no. 5, pp. 2715–2729, Oct. 2021.

[25] Z. Yang, W. Liao, Q. Zhang, C. L. Bak, and Z. Chen, "Fault coordination control for converter-interfaced sources compatible with distance protection during asymmetrical faults," *IEEE Trans. Ind. Electron.*, vol. 70, no. 7, pp. 6941–6952, Jul. 2023.

[26] Z. Yang et al., "Harmonic injection based distance protection for line with converter-interfaced sources," *IEEE Trans. Ind. Electron.*, vol. 70, no. 2, pp. 1553–1564, Feb. 2023.

[27] B. Xia et al., "Estimation of fault resistance using fault record data" *IEEE Trans. Power Del.*, vol. 30, no. 1, pp. 153–160, Feb. 2015.

[28] Z. Wang and L. Mu, "Microgrid fault detection method coordinated with a sequence component current-based fault control strategy," *Prot. Control Mod. Power Syst.*, vol. 9, no. 1, pp. 81–93, Jan. 2024.
[29] K. El-Arroudi et al., "Performance of interconnection protection based on distance relaying for wind power distributed generation," *IEEE Trans. Power Del.*, vol. 33, no. 2, pp. 620–629, Apr. 2018.
[30] A. A. Montanari and A. M. Gole, "Enhanced instantaneous power theory for control of grid connected voltage sourced converters under unbalanced conditions," *IEEE Trans. Power Electron.*, vol. 32, no. 8, pp. 6652–6660, Aug. 2017.
[31] N. Shabanikia and S. A. Khajehoddin, "Weighted dynamic aggregation modeling of grid-following inverters to analyze renewable DG integrated microgrids," *IEEE Trans. Ind. Electron.*, vol. 71, no. 1, pp. 583–594, Jan. 2024.
[32] F. Han et al., "Stability control for grid-connected inverters based on hybrid-mode of grid-following and grid-forming," *IEEE Trans. Ind. Electron.*, vol. 71, no. 9, pp. 10750–10760, Sep. 2024.
[33] P. Chang et al., "A single-terminal fault location method for transmission lines integrated by inverter-type source," *IEEE Trans. Power Del.*, vol. 37, no. 3, pp. 1704–1713, Jun. 2022.
[34] Z. Yang et al., "Control-based faulty phase detection methods for lines with converter-interfaced sources" *IEEE Trans. Ind. Electron.*, vol. 71, no. 7, pp. 7290–7300, Jul. 2024.
[35] X. Gao, G. Song, C. Zhang, X. Kang, and J. Yan, "A novel directional pilot protection of submarine cables for low frequency transmission system with offshore wind power" *IEEE Trans. Power Del.*, vol. 40, no. 1, pp. 273–286, Feb. 2025.
[36] *IEEE Guide for Determining Fault Location on AC Transmission and Distribution Lines*, *IEEE Std C37.114-2014*, Jan. 2015.
[37] G. Song et al., "A phase selection method for wind power integration system using phase voltage waveform correlation" *IEEE Trans. Power Del.*, vol. 32, no. 2, pp. 740–748, Apr. 2017.
[38] B. Patel, "Superimposed components of Lissajous pattern based feature extraction for classification and localization of transmission line faults," *Electr. Power Syst. Res.*, vol. 215, 2023, Art. no. 109007.
[39] J. Zhang et al., "Improved schemes for traditional current-based phase selectors in wind power systems," *IET Gener. Transm. Distrib.*, vol. 12, no. 21, pp. 5781–5788, 2018.
[40] Y. Xie et al., "Improved fault phase selection scheme for lines terminated by inverter based resources," in *Proc. IEEE PES General Meeting (PESGM)*, Orlando, FL, USA, 2023, pp. 1–5.
[41] S. Huang, L. Luo, and K. Cao, "A novel method of ground fault phase selection in weak-infeed side," *IEEE Trans. Power Del.*, vol. 29, no. 5, pp. 2215–2222, Oct. 2014.
[42] A. Jalilian et al., "Distance protection of transmission lines in presence of inverter-based resources: A new earth fault detection scheme during asymmetrical power swings," *IEEE Trans. Ind. Appl.*, vol. 58, no. 2, pp. 1899–1909, Mar./Apr. 2022.
[43] A. dos Santos, C. Gaspar, M. T. C. de Barros, and P. Duarte, "Transmission line fault resistance values based on field data" *IEEE Trans. Power Del.*, vol. 35, no. 3, pp. 1321–1329, Jun. 2020.
[44] L. Zheng et al., "A novel structural similarity based pilot protection for renewable power transmission line," *IEEE Trans. Power Del.*, vol. 35, no. 6, pp. 2672–2681, Dec. 2020.
[45] C. Chao et al., "Collaborative solution of distance protection and dual current control for outgoing lines of inverter-based resources during line-to-line faults," *IEEE Tran. Smart Grid*, vol. 15, no. 4, pp. 3782–3794, Jul. 2024.
[46] E. Afshari et al., "Control strategy for three-phase grid-connected PV inverters enabling current limitation under unbalanced faults," *IEEE Trans. Ind. Electron.*, vol. 64, no. 11, pp. 8908–8918, Nov. 2017.
[47] H. Zhang et al., "Simultaneous overvoltage and overcurrent mitigation strategy of grid-forming inverters under a single-line-to-ground fault," *IEEE Trans. Ind. Electron.*, vol. 71, no. 9, pp. 10818–10830, Sep. 2024.

Yuhao Xie (Student Member, IEEE) received the B.S. degree in electrical and electronic engineering in 2022 from ShanghaiTech University, Shanghai, China, where he is currently working toward the Ph.D. degree in electrical engineering.

His research interests include protection and fault location in the presence of inverter-based resources.

Xinchen Zou (Student Member, IEEE) received the B.S. degree in computer science from Harbin Institute of Technology, Harbin, China, in 2022. He is currently working toward the M.S. degree in electrical engineering with ShanghaiTech University, Shanghai, China.

His research interests include data-driven fault location of power system and power electronic systems.

Mengzhao Duan (Student Member, IEEE) received the B.S. degree in electrical engineering and automation from Dalian University of Technology, Dalian, China, in 2021 and the M.S. degree in electrical and electronic engineering from ShanghaiTech University, Shanghai, China, in 2024. He is currently working toward the Ph.D. degree in electrical engineering with Hong Kong Polytechnic University, Hong Kong, China, with emphasis on power system.

Feilong Fan (Member, IEEE) received the B.E. degree from Zhejiang University, Hangzhou, China, in 2014, and the Ph.D. degree from Shanghai Jiao Tong University, Shanghai, China, in 2019, both in electrical engineering.

Currently, he is an Assistant Professor with Shanghai Jiao Tong University. His research interest includes the energy management of the integrated energy systems.

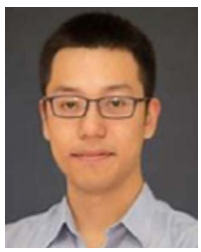

Haoyu Wang (Senior Member, IEEE) received the B.S. degree from Zhejiang University, Hangzhou, China, in 2009, and the Ph.D. degree from the University of Maryland, College Park, MD, USA, in 2014, both in electrical engineering.

Currently, he is a Tenured Full Professor with ShanghaiTech University, Shanghai, China. His research interests include power electronics, plug-in electric and hybrid vehicles, the applications of wide-bandgap semiconductors, and power management integrated circuits.

Dr. Wang is an Associate Editor of IEEE TRANSACTIONS ON INDUSTRIAL ELECTRONICS and IEEE TRANSACTIONS ON TRANSPORTATION ELECTRIFICATION.

Yu Liu (Senior Member, IEEE) received the B.S. and M.S. degrees in electrical power engineering from Shanghai Jiao Tong University, Shanghai, China, in 2011 and 2013, respectively, and the Ph.D. degree in electrical and computer engineering from Georgia Institute of Technology, Atlanta, GA, USA, in 2017.

Currently, he is a Tenured Associate Professor with ShanghaiTech University, Shanghai. He has authored and co-authored more than 130 peer-reviewed research papers in the area of modeling, protection, fault location, and state/parameter estimation of power systems and power electronic systems.

Dr. Liu is an Associate Editor of IEEE TRANSACTIONS ON POWER DELIVERY, *IET Renewable Power Generation*, and *Protection and Control of Modern Power Systems*.